

This is the final peer-reviewed accepted manuscript of:

Roy, M., Berezhnaia, V., Villa, M., Vanthuyne, N., Giorgi, M., Naubron, J.-V., Poyer, S., Monnier, V., Charles, L., Carissan, Y., Hagebaum-Reignier, D., Rodriguez, J., Gingras, M., & Coquerel, Y. (2020). Stereoselective Syntheses, Structures, and Properties of Extremely Distorted Chiral Nanographenes Embedding Hextuple Helicenes. *Angewandte Chemie International Edition*, 59(8), 3264–3271

The final published version is available online at:
<https://doi.org/10.1002/anie.201913200>

Terms of use:

Some rights reserved. The terms and conditions for the reuse of this version of the manuscript are specified in the publishing policy. For all terms of use and more information see the publisher's website.

This item was downloaded from IRIS Università di Bologna (<https://cris.unibo.it/>)

When citing, please refer to the published version.



Stereoselective Syntheses, Structures and Properties of Extremely Distorted Chiral Nanographenes Embedding Hextuple Helicenes

Myriam Roy, Veronika Bereznaia, Marco Villa, Nicolas Vanthuyne, Michel Giorgi, Jean- Valère Naubron, Salomé Poyer, Valérie Monnier, Laurence Charles, Yannick Carissan, et al.

► To cite this version:

Myriam Roy, Veronika Bereznaia, Marco Villa, Nicolas Vanthuyne, Michel Giorgi, et al.. Stereoselective Syntheses, Structures and Properties of Extremely Distorted Chiral Nanographenes Embedding Hextuple Helicenes. *Angewandte Chemie International Edition*, 2020, 59 (8), pp.3264-3271. 10.1002/anie.201913200 . hal-03064338

HAL Id: hal-03064338

<https://hal.science/hal-03064338>

Submitted on 14 Dec 2020

HAL is a multi-disciplinary open access archive for the deposit and dissemination of scientific research documents, whether they are published or not. The documents may come from teaching and research institutions in France or abroad, or from public or private research centers.

L'archive ouverte pluridisciplinaire **HAL**, est destinée au dépôt et à la diffusion de documents scientifiques de niveau recherche, publiés ou non, émanant des établissements d'enseignement et de recherche français ou étrangers, des laboratoires publics ou privés.

Stereoselective Syntheses, Structures and Properties of Extremely Distorted Chiral Nanographenes Embedding Hextuple Helicenes

Myriam Roy,^[a] Veronika Bereznaia,^[a] Marco Villa,^[a] Nicolas Vanthuyne,^[b] Michel Giorgi,^[d] Jean-Valère Naubron,^[d] Salomé Poyer,^[e] Valérie Monnier,^[d] Laurence Charles,^[e] Yannick Carissan,^[b] Denis Hagebaum-Reignier,^[b] Jean Rodriguez,^[b] Marc Gingras,^{*[a]} Yoann Coquerel^{*[b]}

Abstract: We report a molecular design and concept using π system elongation and steric effects from helicenes surrounding a triphenylene core toward stable chiral polycyclic aromatic hydrocarbons (PAHs) with a maximal π distortion to tackle the aromaticity, supramolecular and molecular properties. The selective syntheses, and the structural, conformational and chiroptical properties of two diastereomeric large multihelices of formula $C_{90}H_{48}$ having a triphenylene core and embedding three [5]helicene units on the inner edges and three [7]helicene units at the periphery are reported based on diastereoselective and, when applicable, enantioselective (!) Yamamoto type cyclotrimerizations of racemic or enantiopure 9,10-dibromo[7]helicene. Both molecules have an extremely distorted triphenylene core, and one of them exhibits the largest torsion angle recorded so far for a benzene ring (twist = 36.9°). The analysis of aromaticity distribution in these model molecules using magnetic criteria revealed a nonaromatic character of the triphenylene cores and provides a new look at aromaticity in three-dimensional PAHs. One diastereomer can complex up to three silver(I) ions in the bay region (cavities) of its periphery [7]helicene units, opening the door to chiral catalytic metanano-graphene hybrids.

Introduction

Two-dimensional polycyclic aromatic hydrocarbons (PAHs) are diverse in sizes and shapes, starting from small naphthalene or triphenylene units to graphene sheets and/or flakes having both dimensions larger than 100 nm. Large PAHs can exhibit exceptional electronic and physical properties governed by the

size and the nature of the periphery. Thus, considerable efforts are currently underway to synthesize well-defined large 2D PAHs such as graphene nanoribbons and nanographenes by organic syntheses (bottom up approach) in solution or on a surface and to investigate their properties and applications.^[1] Because PAHs are somewhat flexible and stretchable molecules, it allows the design of curved PAHs such as bowls, saddles, coiled ribbons, propellers and circular belts with defined molecular chirality.^[2] The latter properties of a great interest in life, chemical, and physical sciences as well as technology, because it allows an additional tuning of molecular properties and functions for many applications.^[3] Large chiral PAHs have thus become molecules of utmost interest as three-dimensional chiral nanographenes, and small curved PAHs are now often sought as building blocks for their construction in the racemic series.^[4] In that direction, multihelices have emerged as a class of promising well-defined chiral PAHs.^[5] Multihelices can exist as several diastereomers, each existing as a pair of enantiomers (except in the cases of some achiral *meso* diastereomers), that can more or less rapidly interconvert depending on the torsional energy and flexibility of the molecules. The proper accumulation of helical strain in multihelices can produce exceptionally distorted molecules showing some benzene units suffering from an extreme torsion angle. For instance, record torsions of 35.3° and 35.7° were recently measured in a D_2 symmetric quadrupel helix^[6] and a C_2 symmetric hextuple helix,^[7] respectively. A fruitful approach to racemic triphenylene helices and higher order congeners was based on cyclotrimerization reactions to forge a distorted triphenylene core.^[7,8] Using this approach, we report herein the diastereoselective and, when applicable, enantioselective syntheses of two large and extremely distorted diastereomeric hextuple helices of formula $C_{90}H_{48}$. The conformational behavior, the structure, the chiroptical properties and the torsion induced deficient local aromaticity in these molecules are discussed in detail, together with the exploration of the complexation ability toward silver(I) ions for one of them.

Results and Discussion

Syntheses and conformational properties. It was envisioned that the chiral three blade propeller shaped hextuple helix D_3 **2** of formula $C_{90}H_{48}$ could be prepared by a Yamamoto type cyclotrimerization of 9,10-dibromo[7]helicene **1** (Figure 1a). The

- [a] Dr M Roy Dr M Villa Dr V Bereznaia Prof Dr M Gingras
Aix Marseille Univ CNRS C NAM Marseille France
E-mail marc.gingras@univ-amu.fr
- [b] Dr N Vanthuyne Dr Y Carissan Dr D Hagebaum-Reignier Prof
Dr J Rodriguez Dr Y Coquerel
Aix Marseille Univ CNRS Centrale Marseille iSm2 Marseille
France
E-mail yoann.coquerel@univ-amu.fr
- [c] Dr M Roy
Sorbonne Université CNRS Institut Parisien de Chimie Moléculaire
PCM F-75005 Paris France
- [d] Dr M Giorgi Dr J-V Naubron Dr V Monnier
Aix Marseille Univ CNRS Centrale Marseille FSCM Marseille
France
- [e] Dr S Poyer Prof Dr L Charles
Aix Marseille Univ CNRS CR Marseille France

Supporting information for this article is given via a link at the end of the document

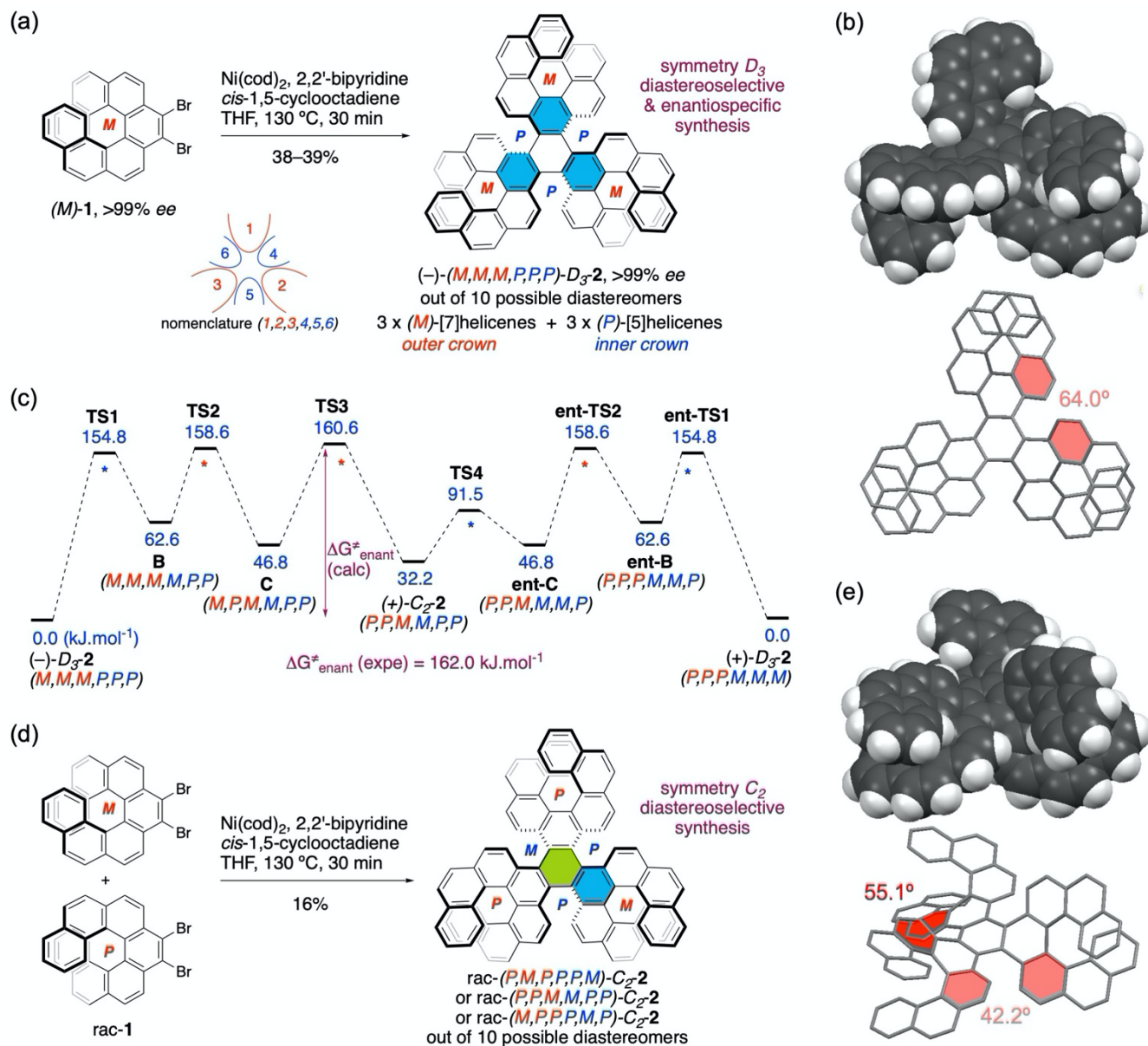


Figure 1. Syntheses and some properties of the hextuple helicenes $(-)-D_3-2$ and $rac-C_2-2$ (a) Yamamoto-type cyclotrimerization of $(M)-9,10$ -dibromo[7]helicene $(M)-1$ leading to $(-)-D_3-2$ (b) Three-dimensional representations of $(-)-D_3-2$ obtained from single-crystal X-ray diffraction analysis (remarkable interplanar angles are highlighted in red) (c) Simplified plausible enantiomerization pathway of D_3-2 obtained by DFT calculations [B3LYP/6-31G(d) in the gas phase] (energies are free Gibbs energies and are expressed in $\text{kJ}\cdot\text{mol}^{-1}$; see the Supporting Information for details) (d) Yamamoto-type cyclotrimerization of racemic 9,10-dibromo[7]helicene ($rac-1$) leading to $rac-C_2-2$ (e) Three-dimensional representations of $rac-C_2-2$ obtained from single-crystal X-ray diffraction analysis (remarkable interplanar angles are highlighted in red).

new chiral PAH embeds three homochiral [7]helicene units on its outer shell and three homochiral [5]helicene units of opposite configuration on its inner edges. [7]Helicene itself has a high barrier to enantiomerization ($178.8 \text{ kJ}\cdot\text{mol}^{-1}$)⁹ precluding its inversion of configuration at a significant rate under the projected reaction conditions (ca. 130 °C). It was assumed that the barriers to inversion of configuration of the various [7]helicene containing species involved in the planned nickel(0) mediated cyclotrimerization would be too high for the synthesis to rely on a thermodynamic control as in previous studies.^{17,8} Thus, it should

be possible to perform the syntheses from enantiopure (*P*) or (*M*) **1** to obtain the corresponding enantiopure hextuple helicene D_3-2 in an enantiospecific manner. Indeed, the nickel(0) mediated cyclotrimerization of (*M*) **1** afforded $(-)-D_3-2$ in a 38% yield (Figure 1a). The same reaction performed with (*P*) **1** gave $(+)-D_3-2$ in a 39% yield (not depicted). Both enantiomers of D_3-2 were thus directly obtained as enantiopure hextuple helicenes, as confirmed by analytical chromatography on a chiral stationary phase. The structure and absolute configuration of $(-)-D_3-2$ were unambiguously

confirmed by single crystal X-ray diffraction methods (Figure 1b) and circular dichroism spectroscopies (see Supporting Information). On a stereochemical point of view, ten diastereomers of **2** are possible: two of C_1 symmetry, six of C_2 symmetry and two of D_3 symmetry. The relative free Gibbs energies were calculated by DFT methods from 0.0 kJ·mol⁻¹ for D_3 **2**, the thermodynamically diastereomer, up to 108.3 kJ·mol⁻¹ for a C_2 symmetric metastable diastereomer. A plausible enantomerization pathway for D_3 **2** was computed with a barrier to enantomerization calculated at 160.6 kJ·mol⁻¹ (Figure 1c), in agreement with a value experimentally determined at 162.0 kJ·mol⁻¹ corresponding to a racemization half-life $t_{1/2}$ = 43 months at 25 °C or 1.3 years at 130 °C. Notably, the barrier to enantomerization of D_3 **2** is lower than for the parent [7]helicene, an oddity for D_n symmetric multi-helicenes in general.^[15] Amusingly, hexuplex helicene D_3 **2** is the second twisted nanographene reported within a short period of time.^[14e] The enantiospecific synthesis of both enantiomers of D_3 **2** from either (*P*) and (*M*) **1** confirmed our hypothesis that no significant inversion of configuration of [7]helicene units can occur at a significant rate in the various synthetic intermediates involved in its synthesis. This translated in a unique opportunity to synthesize diastereoselectively a diastereomer of D_3 **2** from racemic **1**, this time mixing the helices of the [7]helicene units at the outer shell of the molecule. Accordingly, the nucleophilic mediated cyclooligomerization of rac **1** allowed the formation of both the racemic (*PMPMPM*) C_2 **2** and D_3 **2** diastereomers in a 13.8:1 ratio and the isolation of (*PMPMPM*) C_2 **2** in a 16% yield (Figure 1d); note that hexuplex helicene rac (*PMPMPM*) C_2 **2** can also be denominated rac (*PPMMPM*) C_2 **2** or rac (*MPPMPM*) C_2 **2** according to the proposed nomenclature. The structure and relative configurations of rac C_2 **2** were ascertained by single crystal X-ray diffraction analysis (Figure 1e). The free Gibbs energy of diastereomer C_2 **2** was calculated at +32.2 kJ·mol⁻¹ relative to D_3 **2**, and diastereomer C_2 **2** is an intermediate in the computed enantomerization pathway for D_3 **2** (Figure 1c). The enantiomers of diastereomer C_2 **2** were separated by chiral HPLC techniques and were fully characterized by chiroptical methods, including the attribution of the absolute configurations (see the Supporting Information).

Structural and chiroptical studies. The structural features of hexuplex helicenes D_3 **2** and C_2 **2** were carefully examined (Figure 2). The four benzene units from the triphenylene core of D_3 **2** show a marked alternation of bond lengths from 1.404 Å to 1.465 Å (mean values because of the crystallographic C_2 symmetry of D_3 **2**), to be compared to 1.393 Å in benzene, 1.420 Å in graphene, and 1.338 Å and 1.454 Å in 1,3-butadiene,^[10a,b] and may be regarded as the Kekulé structures, i.e. 1,3,5-cyclohexatrienes. The central ring in D_3 **2** exists in a chair conformation and the three surrounding rings adopt severely twisted conformations with a mean torsion angle of 32.4° (Figure 2a). Evaluation of the photophysical properties of D_3 **2** indicated a maximum absorption at 417 nm (ϵ = 90000 M⁻¹cm⁻¹) and maximum emission at 538 nm (quantum yield = 5.7%). The optical rotation

of (*MMPPPP*) D_3 **2** was measured at $[\alpha]_D^{25}$ = 300 (c = 0.0325, CHCl₃), which is an unexpectedly small absolute value when compared to the large optical rotation values of isolated (*P*) [5]helicene ($[\alpha]_D^{25}$ = +1670) and (*M*) [7]helicene ($[\alpha]_D^{25}$ = 5900). Similarly, the electronic and vibrational circular dichroism spectra of D_3 **2** were found of low intensity (see the Supporting Information). It was reasoned that the strong contribution to the chiroptical properties of the three moderately stretched homochiral (*M*) [7]helicene units at the outer shell in (*MMPPPP*) D_3 **2** (mean interplanar angle of the two terminal rings = 39.7° vs 32.3° in [7]helicene tse^{f11a,b}) is somehow compensated by a strong contribution of opposite intensity of the three severely stretched homochiral (*P*) [5]helicene units at its edges (mean interplanar angle of the two terminal rings = 64.0°

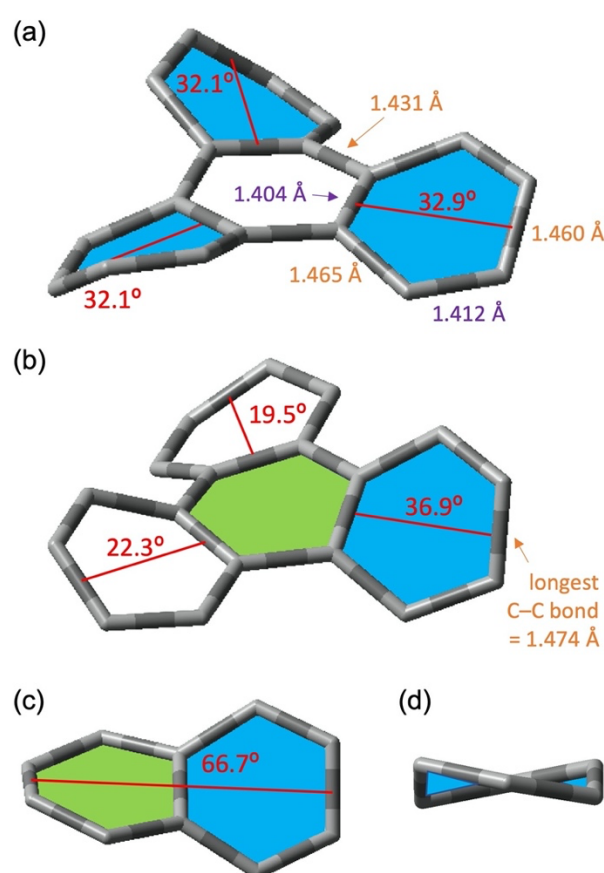


Figure 2. Some structural features of D_3 -**2** and C_2 -**2** (a) The triphenylene core in D_3 -**2** including remarkable torsion angles and bond lengths (mean values). The solid-state conformation of D_3 -**2** has crystallographic C_2 -symmetry justifying for the non-equivalent torsions in all the three blue-colored rings (b) The triphenylene core in C_2 -**2** including remarkable torsion angles and bond length. The solid-state conformation of C_2 -**2** has no crystallographic symmetry justifying for the non-equivalent torsions in the two white-colored rings (c) The naphthalene unit along the molecular C_2 axis in C_2 -**2** showing a very high end-to-end torsion (d) Profile view of the most twisted benzene ring in C_2 -**2**

vs 46.0° in [5]helicene tse^{f11c}). The structural analysis of C_2 **2** also revealed a pronounced bond lengths alternation of the four benzene units from its triphenylene core, with bond lengths

generally comparable with those in D_3 **2**. However, the longest interatomic distance in C_2 **2** is the C–C bond crossed by the C_2 axis in the periphery of the triphenylene core has a length of 1.474 Å (Figure 2b), comparable with the one of the $C(sp^2)$ – $C(sp^2)$ single bond in some biphenyls.^[10c] The C_2 **2** diastereomer was found significantly more distorted than isomer D_3 **2**, with a maximum torsion angle cumulating at 36.9° (!) for the peripheral ring of the triphenylene core on the C_2 axis, establishing the current record of torsion for a “benzene” ring (Figures 2b,d). Also, the naphthalene unit aligned with the C_2 axis in C_2 **2** exhibits a very high end-to-end torsion of 66.7° (Figure 2c, current record = 69.5°^[6]). The optical rotation of (*PMP**PP**M*) C_2 **2** was measured at $[\alpha]_D^{25} = +705$ ($c = 0.0337$, CH_2Cl_2) and its electronic circular dichroism spectrum showed a relatively low intensity (see Supporting Information), chiroptical features comparable with those of diastereomer D_3 **2**. The highly distorted structures of D_3 **2** and C_2 **2** limit the formation of intermolecular π – π interactions, thus allowing enhanced solubility in organic solvents. This is well illustrated by the crystal packing of (*MMMP**PP*) D_3 **2** that shows few interactions between the individual molecules that stack to form supra-helices of (*P*) configuration with in the crystal, creating large chiral CDC₃ solvent channels organized along the *a* and *b* crystallographic axes (Figure 3).

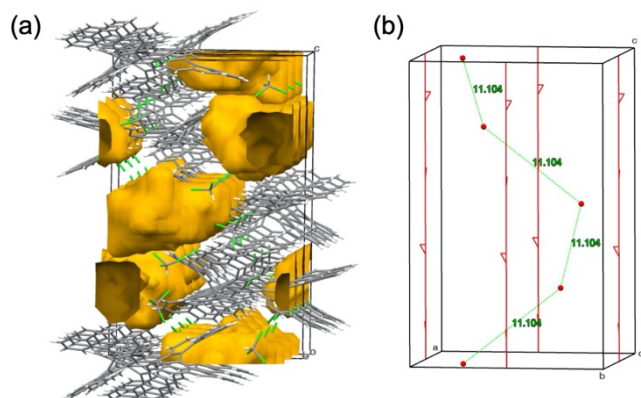


Figure 3. (a) Crystal packing of (*M,M,M,P,P,P*)- D_3 -**2** and representation of the solvent channels along the *b* axis. The content of the channels is a mix of explicitly determined *d*1-chloroform molecules and the calculated mask of solvent (yellow voids) (b) Representation of the (*P*)-configured supra-helix (pitch = crystallographic *c* vector = 27 2785 Å) in the crystal packing of (*M,M,M,P,P,P*)- D_3 -**2**: side view along the *c* axis: the four-fold 4_3 screw axis is in red: the centroids of the central rings of each molecule are represented as red dots and the distances between them (Å) are noted in green

Evaluation of aromaticity. The hexupole helices D_3 **2** and C_2 **2** sustain unprecedented distortion for stable PAHs, pointing out for unusual deficiencies in local aromaticity. Aromaticity is an extremely useful and popular concept in chemistry although there is no single quantitative definition of it, and it is not directly measurable experimentally.^[12] Application of the quantitative Car's rule^[13] to D_3 **2** (or C_2 **2**, stereochemistry is not accounted for in Car's structures) predicts an alternation of local aromaticity with 13 separated π sextets in the Car's structure containing the largest number of disjoint aromatic π sextets (Figure 4d), and nine

disjoint π sextets in the complementary Car's structure. However, the Car's rules strictly valid for planar polycyclic aromatic systems. Structural^[14] energetic^[15] electron density based,^[16] and magnetic based indices^[17] have been developed to characterize and to quantify aromaticity as a property of molecules. However, these indices were also developed for planar systems and their transposition to three-dimensional systems can lead to erratic results. For instance, it was earlier recognized that the popular structural based indices as HOMA (Harmonic Oscillator Model of Aromaticity) and energetic based indices as TRE (Topological Resonance Energy), as well as some electron density based methods, do not perform well for coiled systems as [n]helicenes and can lead to discrepancies.^[18] Indeed, we experienced difficulties with the HOMA during our early work (see Supporting Information). Actually, only magnetic based methods appear applicable to severely twisted aromatics. When an external magnetic field is applied to a molecule, strong induced electron currents are created at aromatic (diatropic currents) and antiaromatic (paratropic currents) rings. The ACID (Anisotropy of the Induced Current Density) method^[19] allows the visualization of an isosurface on which the induced current density vectors are plotted, showing diatropic (clockwise, aromatic) and paratropic (counterclockwise, antiaromatic) currents. However, the method is sensitive to the orientation of the applied external magnetic field, normally perpendicular to the molecular plane, which can be problematic with highly distorted PAHs such as D_3 **2** and C_2 **2**. The NICS (Nucleus Independent Chemical Shifts) index relies on the computation of the local magnetic environment at any desired point in space, often referred to as a ghost atom, and is expressed in ppm.^[20] NICS(0) values refer to ghost atoms placed at the center of each cycle, with large negative NICS(0) probing induced diatropic ring currents attributed to aromaticity. For instance, benzene has a NICS(0) calculated at -8.6 ppm at the level of theory employed herein. Although the combination of both methods allows for a qualitative and quantitative description of the induced electron currents, it should be kept in mind that the connection between induced diatropic ring currents and aromaticity is not straightforward.^[12b, 17]

The NICS analysis of D_3 **2** (Figure 4a) allowed identifying three groups of rings with distinct local aromaticity: (i) the A and B rings of the triphenylene core have NICS(0) values comprised between -0.6 and +0.8 ppm accounting for poorly directed induced ring currents indicating a non-aromatic character of these two rings; (ii) the C and D rings have deficient induced diatropic ring currents with NICS(0) values calculated around -5.3 ppm pointing out for marked deficient local aromaticity; and (iii) the terminal E rings with NICS(0) values of -9.6 ppm denoting full aromaticity. The overestimation of NICS in the terminal rings of [7]helicene is documented and is due to the magnetic coupling with the neighboring ring placed below or above.^[17a] Notably, for each [5]helicene and [7]helicene subunit in D_3 **2** an overall aromaticity than for the parent isolated [5]helicene and [7]helicene was computed (see graphs in Figure 4a). Also, the distribution of local aromaticity in the [7]helicene units in D_3 **2** differs significantly from the one of isolated [7]helicene with the central ring being non-aromatic in D_3 **2**. In order to differentiate torsional effects

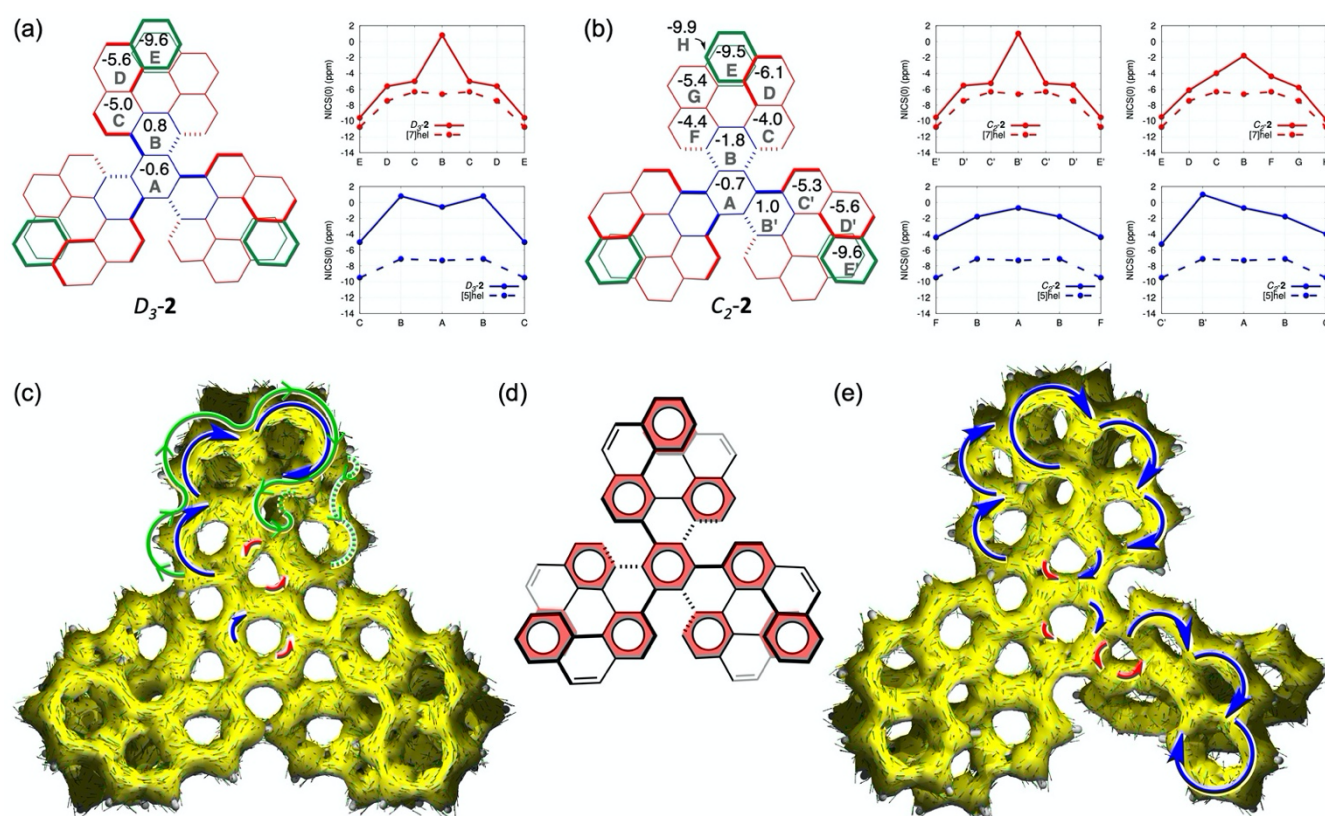


Figure 4. Aromaticity analysis in D_3-2 and C_2-2 (a) NICS(0) values for all non-equivalent rings in D_3-2 . The graphs show the NICS(0) values for the [7]helicene and [5]helicene units in D_3-2 (solid red and blue lines respectively) and isolated [7]helicene and [5]helicene (dashed lines) (b) NICS(0) values for all non-equivalent rings in C_2-2 . The graphs show the NICS(0) values for the [7]helicene and [5]helicene units in C_2-2 (solid red and blue lines respectively) and isolated [7]helicene and [5]helicene (dashed lines) (c) ACID plot of D_3-2 the magnetic field is applied along the +z axis perpendicular to the view plane pointing to the observer diatropic currents are highlighted with blue and green arrows and paratropic currents are highlighted with red arrows (d) Clar's perspective of D_3-2 showing 13 separated π -sextets the Clar's perspective of C_2-2 would be identical (e) ACID plot of C_2-2 the magnetic field is applied along the +z axis perpendicular to the view plane pointing to the observer diatropic currents are highlighted with blue arrows and paratropic currents are highlighted with red arrows

from through space and conjugation effects in the NICS(0) calculations of the triphenylene cores of both D_3-2 and C_2-2 , the NICS(0) were also computed for the virtual triphenylene molecules having the distorted geometries D_3-2 and C_2-2 (see the Supporting Information). Comparison with the NICS(0) of triphenylene itself showed an augmentation of ca. +2 ppm for the distorted rings when compared to the planar counterparts, showing that torsional effects have a significant contribution to the unusual NICS(0) value computed for D_3-2 and C_2-2 . The ACID plot of D_3-2 (Figure 4c) confirmed the NICS analysis: the external rings display clear and strong diatropic ring currents consistent with full aromaticity, the C and D rings exhibit dominant diatropic ring currents but of lower intensity, while the A and B rings show competing small diatropic and paratropic currents indicating weak electron delocalization and a non-aromatic character. The triphenylene core in D_3-2 is probably the least aromatic known triphenylene unit, which correlates with its unprecedented torsion. More globally, a strong diatropic macrocyclic ring current is clearly visible at the periphery of the whole molecular architecture showing global electron delocalization, which is certainly compensating for the severe distortions of the π systems and contributing to the thermodynamic stability. The analysis of local

aromaticity in diastereomer C_2-2 revealed comparable features to the one of D_3-2 with however a more complex situation due to the lower symmetry of the molecule (Figures 4b,e). Notably, the two homochiral [7]helicene units (those not crossed by the C_2 axis) and the triphenylene core have different NICS(0) values. The ACID plot of C_2-2 confirmed qualitatively its overall distorted but of local aromaticity. Altogether, the molecules D_3-2 and C_2-2 are PAHs whose local aromaticity is subjected to variations of large amplitudes from entirely aromatic at the edges to non-aromatic at the cores, correcting the distortion of distortion in the molecules.

Complexation properties of multi-helicene D_3-2 .

[7]Helicene itself was earlier demonstrated to behave as a chiral molecular tweezer for several ions, the meta-cation being sandwiched between the two outermost bonds of the helicene (C3-C4).^[21] It was hypothesized that hexuplex helicene D_3-2 embedding three dendritic and moderately stretched [7]helicene units on its outer shell could behave as a mono, bis or tripe tweezer capable of complexing up to three several ions to form some organic chiral catenation meta-nanographene hybrids (Figure 5). The binding energies for the teratve complexation of one, two

and three *syn* (l) ones inside the bay region of three [7]helicene units in **D₃-2** were evaluated by DFT calculations and compared to the one of Ag⁺ with [7]helicene^[21] (see the Supporting Information). This mode study indicated a slightly better



Figure 5. Computationally optimized structures of the most stable mono-, bis- and triscationic Ag⁺ complexes of **D₃-2** (DFT wB97XD/Def2TZVP//wB97XD/Def2SVP, gas phase). Left: [Ag⊂**D₃-2**]⁺, middle: [2Ag⊂**D₃-2**]²⁺, right: [3Ag⊂**D₃-2**]³⁺.

stabilization for [Ag⊂**D₃-2**]⁺ than for [Ag⊂[7]helicene]⁺, and also that triscatation [3Ag⊂**D₃-2**]³⁺ should be reasonably stable. Experimentally, a methanol/dichloromethane solution of **D₃-2** and AgNO₃ (1:1) was analyzed by electrospray ionization mass spectrometry (ESI-MS) using very soft conditions, drastically limiting the generation of ions upon collision in the interface of the mass spectrometer (i.e. in the gas phase), so that most, if not a, observable results from the electrospray of cationic species naturally present in solution. The formation of both the cation [Ag⊂**D₃-2**]⁺ and the bis-cation [2Ag⊂**D₃-2**]²⁺ in the solution could be clearly evidenced. However, performing ion mobility separation (IMS) prior to mass analysis to further enhance the dynamic range of detection permitted to evidence that [3Ag⊂**D₃-2**]³⁺ is also a stable complex. The relative stability of the three *syn* adducts was evaluated by the 11.2:100:3.8 abundance ratio measured for [Ag⊂**D₃-2**]⁺ / [2Ag⊂**D₃-2**]²⁺ / [3Ag⊂**D₃-2**]³⁺ by IMS-MS, clearly showing the bis-cation [2Ag⊂**D₃-2**]²⁺ complex as the most stable one when observed as naked gas phase ions. The actual reasons for this preference remain unclear at this stage and may include the existence of a more compact and better adjusted conformation for bis-cation [2Ag⊂**D₃-2**]²⁺ than for its mono- and triscatation analogues as seemingly indicated by the experimental determination of collision cross sections (see Supporting Information).

Conclusions

The molecular design and conceptual π system elongation and steric effects, based on helical strands surrounding a triphenylene core with configurational stability [7]helicenes, has led to extreme distortion in some chiral PAHs. This idea was put into practice through a ncked (0) mediated cycloolmerization of enantiopure and racemic 9,10-dibromo[7]helicene, which diastereoselectively afforded large chiral hextuple helices of formula C₉₀H₄₈ with *D₃* and *C₂* symmetry, respectively. The diastereomer with *D₃* symmetry is a three-baded propeller-shaped chiral nanographene that embeds three homochiral [7]helicene units on its outer shell and three homochiral [5]helicene units of opposite configuration on its inner edges. Both *D₃* symmetric enantiomers were directly obtained as enantiopure materials by an enantiospecific Yamamoto-type cycloolmerization, a premise for large chiral

PAHs, and a first example for this type of cycloolmerization. The structural analysis of this molecule revealed a highly distorted triphenylene core with a marked bond lengths alternation of the six-membered rings. The diastereomer with *C₂* symmetry embeds three [7]helicene units of mixed helicity on its outer shell, and three [5]helicene units of mixed helicity on its inner edges so that four (*P*) configured and two (*M*) configured helices are present in the molecule. Its structural analysis also enlightened a pronounced alternation of bond lengths in its triphenylene core, and more remarkably extreme torsions establishing new motifs for benzene (twist = 36.9°). The chiroptical properties of the two hextuple helices were found of relatively small magnitude, possibly due to a phenomenon of compensation between the intertwined (*P*) and (*M*) configured helices. Aromaticity was computationally analyzed in these fascinating molecules using several methods, which was complicated not only because the quantification of the concept of aromaticity is intrinsically difficult, but also because existing models of aromaticity were developed for planar PAHs. Nevertheless, magnetic based methods known as NICS and ACID proved to be useful, though not ideal, and they revealed a non-aromatic character of the triphenylene cores in both diastereomeric hextuple helices, in correlation to the severe distortion of the rings. An early exploration of the metal ions avidity and supramolecular properties of the *D₃* symmetric diastereomer revealed its ability to bind up to three *syn* (l) ions in the bay regions (cavities) of three [7]helicene units at its outer shell, as evaluated by the combination of DFT simulations with advanced mass spectrometry methods, opening the door to the field of chiral cationic meta-nanographene hybrids. To sum up, the present study pushes the limits on the design and the synthesis of highly distorted chiral PAHs, where chirality provides additional control on molecules for modulating their properties for applications in chemistry and materials science. It also deepens the knowledge on the conformation, chiroptical and supramolecular properties (solid and solution states) of chiral PAHs and nanographenes, and raises questions about aromaticity in these large distorted molecules.

Experimental Section

Detailed experimental procedures for the syntheses of (–)-**D₃-2** (+)-**D₃-2** and *rac*-**C₂-2**, the resolution of *rac*-**C₂-2** by HPLC methods, the spectroscopic, structural, chiroptical and photophysical characterization of all compounds, the experimental and computational enantiomerization study of **D₃-2**, the full-detail analysis of aromaticity in **D₃-2**, **C₂-2** and related molecules, the full-detail complexation study of silver(I) cations with **D₃-2** and the crystallographic data for (–)-(*M,M,M,P,P,P*)-**D₃-2** (CCDC 1835903) and *rac*-(*P,M,P,P,P,M*)-**C₂-2** (CCDC 1902495) are included as supporting information for this article.

Acknowledgements

We thank Mrs. R. Rosas (Aix-Marseille Univ.) and Mrs. C. Trouffard (Sorbonne Univ.) for assistance with NMR spectroscopy, Prof. Dr. P. Ceron (Univ. of Bourgogne) for assistance with photophysics, Mrs. M. Jean (CNRS) for assistance with HPLC, and the Centre Régional de Compétences

en Modé sat on Mo écu a re (A x Marse e Un v.) for comput ng fac t es. F nanc a support from a CNRS PICS (No.PICS07573) w th the Un vers ty of Bo gna, the French Ita an Un vers ty for a doctora contract to M.V. (No C2 141 V nc program), AMIDEX (Pyrenex, A M AAP EI 17 171 170301 11.50 GINGRAS SAT), A x Marse e Un vers té and the Centre Nat ona de a Recherche Sc ent f que (CNRS) s gratefu y acknow edged.

Keywords: he cenes • po ycyc c aromat c hydrocarbons • stereose ect v ty • stra ned mo ecu es • aromat c ty

- [1] a) A Narita X-Y Wang X Feng K Müllen *Chem Soc Rev* **2015** 44 6616 b) X-Y Wang A Narita K Müllen *Nat Rev Chem* **2017** 2 100
- [2] Reviews a) M Rickhaus M Mayor M Juriček *Chem Soc Rev* **2016** 45 1542 b) M Rickhaus M Mayor M Juriček *Chem Soc Rev* **2017** 46 1643 c) M A Majewski M Stępień *Angew Chem Int Ed* **2019** 58 86 d) Y Segawa H to K tami *Nat Rev Mats* **2016** 1 15002 e) M Gingras *Chem Soc Rev* **2013** 42 968 f) M Gingras G Felix R Peresutti *Chem Soc Rev* **2013** 42 1007 g) M Gingras *Chem Soc Rev* **2013** 42 1051 h) Y Shen C-F Chen *Chem Rev* **2012** 112 1463 i) M Ball Y Zhong Y Wu C Schenck F Ng M Steigerwald S Xiao C Nuckolls *Acc Chem Res* **2015** 48 267 j) A Bedi O Gidron *Acc Chem Res* **2019** 52 2482 Selected recent reports k) K Y Cheung C K Chan Z Liu Q Miao *Angew Chem Int Ed* **2017** 56 9003 l) M Daigle D Miao A Lucotti M Tommasini J-F Morin *Angew Chem Int Ed* **2017** 56 6213 m) C M Cruz S Castro-Fernández E Maças J M Cuerva A G Campaña *Angew Chem Int Ed* **2018** 57 14782 n) Y Nakakuki T Hirose H Sotome H Miyasaka K Matsuda *J Am Chem Soc* **2018** 140 4317 o) G Povie Y Segawa T Nishihara Y Miyauchi K tami *J Am Chem Soc* **2018** 140 10054 p) G R Kiel S C Patel P W Smith D S Levine T D Tilley *J Am Chem Soc* **2017** 139 18456 q) N J Schuster R H Sánchez D Bukharina N A Kotov N Berova F Ng M Steigerwald C Nuckolls *J Am Chem Soc* **2018** 140 6235
- [3] J R Brandt F Salerno M J Fuchter *Nat Rev Chem* **2017** 1 45
- [4] a) J M Fernández-García P J Evans S M Rivero Fernández D García-Fresnadillo J Perles J Casado N Martín *J Am Chem Soc* **2018** 140 17188 b) K Kato Y Segawa L T Scott K tami *Angew Chem Int Ed* **2018** 57 1337 c) P J Evans J Ouyang L Favereau J Crassous Fernández J Perles N Martín *Angew Chem Int Ed* **2018** 57 6774 d) T Fujikawa D V Preda Y Segawa K tami L T Scott *Org Lett* **2016** 18 3992 e) C M Cruz R Márquez S Castro-Fernández J M Cuerva E Maças A G Campaña *Angew Chem Int Ed* **2019** 58 8068 f) D Meng C Liu C Xiao Y Shi L Zhang L Jiang K K Baldrige Y Li J S Siegel Z Wang *J Am Chem Soc* **2019** 141 5402
- [5] Reviews a) C Li Y Yang Q Miao *Chem Asian J* **2018** 13 884 b) K Kato Y Segawa K tami *Synlett* **2019** 30 370 For other multi-helicenes c) A Pradhan P Dechambenoit H Bock F Durola *J Org Chem* **2013** 78 2266 d) Y Chen T Marszalek T Fritz M Baumgarten M Wagner W Pisula L Chen K Müllen *Chem Commun* **2017** 53 8474 e) Y Zhu Z Xia Z Cai Z Yuan N Jiang T Li Y Wang X Guo Z Li S Ma D Zhong Y Li J Wang *J Am Chem Soc* **2018** 140 4222 f) Y Wang Z Yin Y Zhu J Gu Y Li J Wang *Angew Chem Int Ed* **2019** 58 587 g) H-A Lin K Kato Y Segawa L T Scott K tami *Chem Sci* **2019** 10 2326 h) K Kawai K Kato L Peng Y Segawa L T Scott K tami *Org Lett* **2018** 20 1932 i) R Yamano Y Shibata K Tanaka *Chem Eur J* **2018** 24 6364 j) Y Zhu X Guo Y Li J Wang *J Am Chem Soc* **2019** 141 5511 k) During the evaluation process of this manuscript Ravat and coworkers also reported the enantiospecific synthesis of ()-D₃-**2** from ()-9 10-dibromo[7]helicene using the nickel-mediated Yamamoto cyclotrimerization that we previously made use of (see ref [8f]) F Zhang E Michail F Saal A-M Krause P Ravat *Chem Eur J* DOI 10.1002/chem.201904962 For cyclohelices see l) A Robert P Dechambenoit E A Hillard H Bock F Durola *Chem Commun* **2017** 53 11540 m) G Naulet L Sturm A Robert P Dechambenoit F Röhricht R Herges H Bock F Durola *Chem Sci* **2018** 9 8930 n) A Robert G Naulet H Bock N Vanthuyne M Jean M Giorgi Y Carissan C Aroulanda A Scalabre E Pouget F Durola Y Coquerel *Chem Eur J* **2019** 25 14364
- [6] T Fujikawa Y Segawa K tami *J Am Chem Soc* **2016** 138 3587
- [7] T Hosokawa Y Takahashi T Matsushima S Watanabe S Kikkawa Azumaya A Tsurusaki K Kamikawa *J Am Chem Soc* **2017** 139 18512
- [8] a) L Barnett D M Ho K K Baldrige R A Pascal Jr *J Am Chem Soc* **1999** 121 727 b) D Peña D Pérez E Guitián L Castedo *Org Lett* **1999** 1 1555 c) D Peña A Cobas D Pérez E Guitián L Castedo *Org Lett* **2000** 2 1629 d) M A Bennett M R Kopp E Wenger A C Willis *J Organomet Chem* **2003** 667 8 e) A Pradhan P Dechambenoit H Bock F Durola *Angew Chem Int Ed* **2011** 50 12582 f) V Bereznaia M Roy N Vanthuyne M Villa J-V Naubron J Rodriguez Y Coquerel M Gingras *J Am Chem Soc* **2017** 139 18508 g) R Zuzak J Castro-Esteban P Brandimarte M Engelund A Cobas P Piątkowski M Kolmer D Pérez E Guitián M Szymonski D Sánchez-Portal S Godlewski D Peña *Chem Commun* **2018** 54 10256 h) Pozo E Guitián D Pérez D Peña *Acc Chem Res* **2019** 52 2472
- [9] R H Martin M J Marchant *Tetrahedron* **1974** 30, 347
- [10] a) F H Allen O Kennard D G Watson L Brammer A G Orpen R Taylor *J Chem Soc, Perkin Trans 2* **1987** S1 b) N C Craig P Groner D C McKean *J Phys Chem A* **2006** 110 7461 c) G Casalone A Gavezzotti M Simonetta *J Chem Soc, Perkin Trans 2* **1973** 342
- [11] a) P T Beurskens G Beurskens T E M van den Hark *Cryst Struct Comm* **1976** 5 241 b) T E M van den Hark P T Beurskens *Cryst Struct Comm* **1976** 5 247 c) R Kuroda *J Chem Soc Perkin Trans 2* **1982** 789
- [12] a) For the definition of aromaticity by UPAC see <https://goldbook.iupac.org/html/A/A00442.html> b) A Stanger *Chem Commun* **2009** 1939 c) J Grunenberg *Int J Quant Chem* **2017** 117 e25359
- [13] M Solá *Front Chem* **2013** 1 22
- [14] T M Krygowski H Szatylowicz O A Stasyuk J Dominikowska M Palusiak *Chem Rev* **2014** 114 6383
- [15] a) M K Cyrański *Chem Rev* **2005** 105 3773 b) J-i Aihara *Bull Chem Soc Jpn* **2016** 89 1425
- [16] F Feixas E Matito J Poater M Solá *Chem Soc Rev* **2015** 44 6434
- [17] R Gershoni-Oranne A Stanger *Chem Soc Rev* **2015** 44 6597
- [18] a) G Portella J Poater J M Bofill P Alemany M Solá *J Org Chem* **2005** 70 2509 b) H Kalam A Kerim K Najmidin P Abdurishit T Tawar *Chem Phys Lett* **2014** 592 320 c) D W Szczepanik M Andrzejak J Dominikowska B Pawetek T M Krygowski H Szatylowicz M Solá *Phys Chem Chem Phys* **2017** 19 28970
- [19] a) D Geuenich K Hess F Köhler R Herges *Chem Rev* **2005** 105 3758 b) R Herges Magnetic Properties of aromatic compounds and aromatic transition states in The Chemical Bond Chemical Bonding Across the Periodic Table (Frenking G Shaik S Eds) Wiley-VCH-Verlag 2014
- [20] Z Chen C S Wannere C Corminboeuf R Puchta P von R Schleyer *Chem Rev* **2005** 105 3842
- [21] a) M J Fuchter J Schaefer D K Judge B Wardzinski M Weimar Krossing *Dalton Trans* **2012** 41 8238 b) E Makrík B Klepetářová D Sýkora S Böhm P Vaňura J Storch *Chem Phys Lett* **2015** 635 355